Check for updates

RESEARCH ARTICLE

Aspiration-induced orthotopic lung cancer model: a non-invasive method for *in vivo* tumor microenvironment studies

[version 1; peer review: 1 approved with reservations]

Müge Özkan[1], İrem Evcili[1], Bilgi Güngör[1,2]

[1]BG Immune Modulation Lab, Izmir Biomedicine and Genome Center, Izmir, 35340, Turkey
[2]Izmir Biomedicine and Genome Institute, Dokuz Eylul University, Izmir, 35340, Turkey

v1 **First published:** 10 Sep 2026, **6**:340
https://doi.org/10.12688/openreseurope.24932.1
Latest published: 10 Sep 2026, **6**:340
https://doi.org/10.12688/openreseurope.24932.1

Abstract

Background

Solid tumors account for the majority of cancer-associated morbidity, and the tumor microenvironment (TME) is a critical determinant of therapeutic response. However, the limited availability of optimized preclinical orthotopic cancer models that allow investigation of the TME constrains the development and evaluation of novel treatment approaches.

Methods

Here, we establish a non-invasive orthotopic lung cancer (OLC) model based on aspiration-mediated inoculation of luciferase-expressing Lewis lung carcinoma (LL2-luc2) cells, compared with the intranasal (i.n.) inoculation method. We monitored tumor progression weekly using *in vivo* bioluminescence imaging (BLI) and conducted welfare checks three times per week. We used endpoint histopathological analysis to validate tumor establishment and quantify tumor burden. Furthermore, we analyzed the tumor microenvironment (TME), to assess immune cell distribution and infiltration into the tumor.

Results

Inoculation of LL2-luc2 cells via aspiration resulted in consistent tumor engraftment across animals (6/6), with a defined humane endpoint between days 33–40 post-inoculation. Although the BLI signal enabled monitoring of established tumors, its quantitative correlation with histological tumor burden was limited. Analyzing lungs by immunofluorescence, we found that immune cells localized at the

Open Peer Review

Approval Status ?

	1
version 1 10 Sep 2026	? view

1. **Ho Wan Chan**, The University of Hong Kong, Pokfulam, China
King's College London Institute of Pharmaceutical Science (Ringgold ID: 206990), London, UK

Any reports and responses or comments on the article can be found at the end of the article.

tumor borders, demonstrating a spatial distribution of $CD3^+$ and $MHCII^+$ cells consistent with an immune-excluded-like microenvironment.

Conclusions

Together, our findings support the use of aspiration-based LL2-luc2 inoculation as a practical approach for studying tumor-microenvironment interactions.

Keywords
Orthotopic, lung cancer, aspiration, TME



This article is included in the Horizon Europe gateway.



This article is included in the Marie-Sklodowska-Curie Actions (MSCA) gateway.

Corresponding authors: Müge Özkan (muge.ozkan@ibg.edu.tr), Bilgi Güngör (bilgi.gungor@ibg.edu.tr)

Author roles: Özkan M: Conceptualization, Formal Analysis, Investigation, Methodology, Validation, Visualization, Writing – Original Draft Preparation; **Evcili İ**: Investigation, Writing – Review & Editing; **Güngör B**: Conceptualization, Supervision, Writing – Review & Editing

Competing interests: No competing interests were disclosed.

Grant information: This project has received funding from the [European Union's Horizon Europe research and innovation programme] under the Marie Skłodowska-Curie grant agreement No [101126492]. The research was funded by 2236-B Marie Sklodowska-Curie Actions (MSCA) Cofund Scholarship Programs Contribution Fund Program (TUBITAK project ID: 123C460).
The funders had no role in study design, data collection and analysis, decision to publish, or preparation of the manuscript.

Copyright: © 2026 Özkan M *et al*. This is an open access article distributed under the terms of the Creative Commons Attribution License , which permits unrestricted use, distribution, and reproduction in any medium, provided the original work is properly cited.

How to cite this article: Özkan M, Evcili İ and Güngör B. **Aspiration-induced orthotopic lung cancer model: a non-invasive method for *in vivo* tumor microenvironment studies [version 1; peer review: 1 approved with reservations]** Open Research Europe 2026, **6**:340 https://doi.org/10.12688/openreseurope.24932.1

First published: 10 Sep 2026, **6**:340 https://doi.org/10.12688/openreseurope.24932.1

Introduction

Preclinical cancer models are essential for understanding tumor biology and developing diagnostic and therapeutic strategies. These aims can only be achieved by a realistic model that is able to recapitulate not only tumor expansion and metastasis, but also the interaction of the tumor with the environment.[1,2] Orthotopic tumor models accurately replicate tumor vascularization, hypoxia, extracellular matrix architecture, immune suppression, and poor immune cell infiltration[1] that are hallmarks of challenging human cancers. Several studies compared subcutaneous and orthotopic colon[3] and (HPV)-positive oropharyngeal squamous cell carcinoma (OSCC)[4] tumor models to evaluate immune cell distribution, infiltration into the tumor, and response to therapies. Specifically, subcutaneous OSCC showed complete survival, whereas survival in the orthotopic model declined as the tumor progressed.[4] The immune cell infiltration patterns differed between subcutaneous and orthotopic tumors, with the orthotopic tumor showing a gradual decline in T cell infiltration, consistent with immune-excluded tumor cases observed in humans.[4] Similarly, Snipstad *et al.*[3] compared the characteristics of different colon cancer cell lines in subcutaneous and orthotopic tumor models and reported that subcutaneous tumors have a significantly increased frequency of infiltrating $CD8^+$ and $CD4^+$ T cells, as well as NK cells, associated with a more immunoreactive phenotype. In both studies, orthotopic tumors did not respond to anti-PD1 treatment, whereas subcutaneous tumors showed modest increases in immune cell infiltration following therapy.[3,4]

Lung cancer remains one of the leading causes of cancer-related mortality worldwide[5] with a 5-year survival rate below 30%.[6] Immune checkpoint inhibitors (ICIs) are common treatment options, however, resistance to ICIs is frequently characterized by an immunosuppressive tumor microenvironment that limits therapeutic response.[7] Immune-excluded or poorly infiltrated phenotypes in lung tumors are common.[7] Studies analyzing patient samples from non-small cell lung cancer found that B-cell and T-cell infiltration into the tumor was associated with improved survival[8] and that clusters of B and/or T cells at the tumor borders were linked to poor survival.[9] Therefore, preclinical models that accurately reflect the spatial and immune architecture of lung tumors are essential for understanding TME interactions and for developing effective therapeutic strategies.

Establishing reproducible lung tumors in preclinical models remains technically challenging.[10] Genetically engineered murine models (GEMM),[11,12] humanized mouse models,[12] human xenograft models,[13,14] and syngeneic immunocompetent models[12] are commonly used to establish orthotopic tumors in the preclinical setting. There are advantages and limitations to each system. GEMMs alone can only mimic specific oncogenic features of the tumor and are costly.[11] Humanized murine and human xenograft models allow engraftment of tumors derived from clinical samples. Still, these experimental models usually rely on immunodeficient mice, with either no or partially reconstituted immune systems, which prevents investigation of tumor-immune system interactions and immune responses observed in patients.[2,11,12] Syngeneic orthotopic models rely on engrafting murine cancer cells into an immunocompetent murine host. This reduces costs and ensures consistency across the experimental platform needed for preclinical experiments.[12] In addition to their advantages, orthotopic syngeneic cancer models have two major limitations: a variable inoculation success rate (60–100%) and a requirement for technical/surgical expertise. Reported inoculation success rates for orthotopic cancer models in the lung,[15] breast,[16] and colorectal[17] are 67% to 100%, and higher success is often associated with invasive surgical engraftment, which usually relies on site-directed injection of tumor cells.[18]

Intratracheal and intrapulmonary injections are common approaches for the delivery of tumor cells into the lung, but[19,20] require surgical intervention and technical expertise, introduce operator-dependent variability, and carry a higher risk of local tissue injury that alters tumor–microenvironment interactions.[18,19] Therefore, minimally invasive methods are necessary to achieve more reproducible and consistent results.[20,21] Accordingly, systemic delivery by intravenous injection,[22] pulmonary delivery routes such as intranasal[23] and oropharyngeal administration,[24] widely used for delivering infectious material or biologics directly to the lung, are attractive minimally invasive alternatives. Unlike non-invasive intratracheal instillation, aspiration does not require direct visualization or cannulation of the trachea and instead relies on spontaneous inhalation of the inoculum delivered to the oropharynx.

Recent work has adopted intranasal delivery for orthotopic lung tumor establishment, providing a non-invasive alternative that more closely reflects tumor initiation in alveolar regions.[15] However, variability in tumor engraftment efficiency, progression, and size within experimental groups remains a challenge. Oropharyngeal aspiration is widely used in pulmonary research to achieve uniform delivery of biologics to the distal lung.[24] Yet whether this approach can reliably deliver viable tumor cells to establish orthotopic lung tumors has not been investigated. Consequently, there is currently no validated aspiration-based orthotopic lung cancer model for studies of tumor progression and the tumor microenvironment.

In this study, we developed and characterized an aspiration-based, non-invasive model for orthotopic lung cancer in immunocompetent mice. We directly compared the aspiration route with intranasal delivery and evaluated tumor

establishment, longitudinal progression, and the spatial immune cell distribution within the TME. Our findings demonstrate that aspiration enables consistent tumor establishment and disease progression, while mimicking a tumor microenvironment with limited intratumoral immune cell infiltration. This provides a practical approach for *in vivo* studies of lung tumor–microenvironment interactions.

Methods

Animals

The C57BL/6 mice were originally obtained from the Jackson Laboratory (JAX, Strain ID:000664). Wild-type C57BL/6 animals that were 7–8 weeks old, from both female and male sexes (control = 2F/3M, i.n. = 5F/1M and aspiration = 5F/1M), were included throughout the study. Animals were housed in the vivarium at the Izmir Biomedicine and Genome Center (IBG, Izmir, Turkey) in compliance with the relevant institutional animal care and use committee guidelines and applicable national laws. *In vivo* experiments were performed with prior approval by the institutional ethics committee (Izmir Biomedicine and Genome Center's internal Ethical Committee on Animal Experimentation, protocol #: 2025–007), in accordance with national laws and Directive 2010/63/EU. The sample size was calculated according to the 3R rule and the experience of the lead researcher. Mice were randomly allocated to the experimental groups before inoculation and assigned individual identification numbers at the time of inoculation. Researchers were not blinded during experimental procedures or data analysis. Mice that lost more than 20% of their body weight and/or scored 3 points on the 5-point scoring system adapted from the murine sepsis scoring system[25] were euthanized. Euthanasia was performed by cervical dislocation under aseptic conditions and in designated areas in accordance with Institute regulations. Death was confirmed by the absence of respiration and lack of response to the toe pinch reflex.

Luciferase-conjugated lewis lung cancer cell maintenance and storage

Luciferase-conjugated Lewis Lung Cancer (LL2-luc2) was purchased from ATCC (CRL-1642-LUC2, Europe). LL2-luc2 was revived according to the manufacturer's guidelines. Cells were cultured under sterile conditions with complete Dulbecco's Modified Eagle's Medium with high Glucose (Serana, Germany) supplemented with 10% FBS (v/v) (Biological Industries, USA) 4 mM L-glutamine (Sartorius, USA), 4500 mg/L glucose, 1 mM sodium pyruvate (Sartorius, USA), and Blasticidin (2 ug/mL) (Invivogen, USA). Once the confluence reached 80%, cells were lifted by Trypsin-EDTA for 1 min at 37 °C. 2 mL Trypsin-EDTA (Biological Industries, USA) was deactivated with 1:10 (v/v) complete medium and centrifuged at 100 g for 5 min. Cells were washed twice and subcultured at a 1:4 dilution three times per week. Before inoculation into animals, cells were detached as described previously. Cells were washed twice with 15 mL PBS (Sartorius, USA) and counted using a hemacytometer. Cell concentration was adjusted to 10^6 live cells per 50 µl (20×10^6 cells/mL) and kept on ice.

In vivo orthotopic lung cancer model

Prior to inoculation, the luciferase activity of LL2-luc2 cells was verified *in vitro*. Wild-type C57BL/6 mice were randomly assigned to the following groups: intranasal PBS control, aspiration PBS control, intranasal LL2-luc2 inoculation (n = 6), and aspiration LL2-luc2 inoculation (n = 6). For tumor inoculation, animals were anesthetized with isoflurane (Adeka İlaç Sanayi Ve Ticaret A.Ş.,Türkiye) and 10^6 LL2-luc2 cells in 50 µL PBS were administered via aspiration as previously described.[26] Briefly, the mouse was stabilized on a tilted stage via its incisors, the tongue was gently lifted laterally using sterile blunt-end forceps, and the cell suspension was instilled into the pharyngeal/laryngeal region via a P200 pipette. Upon spontaneous inhalation, the inoculum was aspirated into the lungs. For intranasal inoculation, 10^6 LL2-luc2 cells in 50 µL PBS were administered dropwise onto the nostrils of anesthetized mice, allowing passive inhalation. The control group received 50 µL PBS via either aspiration or intranasal delivery following the same procedures.

The mice were weighed and monitored every 2 days. Tumor progression was assessed by weekly *in vivo* bioluminescence measurements. The humane endpoint was determined by a scoring system adapted from the murine sepsis scoring system, where appearance, behavior, respiratory function, body weight change were evaluated. Mice that lost >20% from baseline weight, showed persistent moderate to severe scores for more than 24 hours (any parameter or combined score ≥ 3), has labored breathing or gasping (respiratory function score ≥ 3), could not eat/drink themselves, were unresponsive or lethargic, or had an abnormal condition such as cyanosis or vaginal/cervical hyperplasia were euthanized immediately. The experiment was concluded once all mice that were inoculated via aspiration reached the humane endpoint, day 40 post-inoculation. At day 33, three control and two intranasally inoculated mice were euthanized for matched terminal tissue collection when three aspiration-inoculated animals began reaching the predefined humane endpoint. Consequently, longitudinal measurements from these animals were included through day 33, and subsequent analyses included only animals remaining in the study.

In vivo bioluminescence imaging

Bioluminescence imaging was performed to monitor tumor progression *in vivo.* Mice were injected intraperitoneally with D-luciferin (Revvity, Netherlands) prepared according to the manufacturer's instructions, at a dose of 150 mg/kg. Mice were anesthetized with isoflurane. Imaging was initiated 10 minutes after the D-luciferin injection (MILabs, The Netherlands).

For each imaging session, images were acquired sequentially at 2-minute intervals for 15 minutes. Identical acquisition parameters: 45-second exposure, 2X gain, and 4x4 binning were applied across all animals and imaging sessions. The signal corresponding to the orthotopic lung tumor was quantified from a thoracic region of interest (ROI) as integrated electron flux using MILabs software, which provides background-subtracted and sensitivity-adjusted values.

Histology

Lungs were inflated with 1 mL 10% neutral buffered formaldehyde (Tekkim, Türkiye) and fixed for four hours at 4 °C. Lungs were dehydrated in 20 mL 30% sucrose (Sigma-Aldrich, Germany) overnight at 4 °C, embedded in cryomolds (Tissue-Tek, Sakura, USA) with O.C.T. (Tissue-Tek, Sakura, US) the following day (15 hours later), and snap-frozen. Serial sections in 10–15 µm thickness were prepared using a cryostat (Leica CM1950). Digital pathology analysis was performed on the section containing the largest visible tumor area to ensure consistent comparison between animals. H&E staining was performed as a service by IBG's Histopathology Core Facility according to its routine protocol as previously described.[26] Samples were mounted and examined with a light microscope (Olympus BX61).

Immunofluorescence

The tissue sections were stored at −20 °C until use. Prior to staining, slides were kept at RT and rehydrated in PBS for 10 min. The sample borders were drawn by the PAP pen (Sigma-Aldrich, Germany). Then, the slides were blocked in a buffer containing 2% BSA (Capricorn, USA) and 0.01% Triton X-100 (Sigma-Aldrich, Germany). Samples were stained with CD3-AF647(clone 17A2, 1:100, BD Biosciences, USA), MHCII-PE (clone: M5/114.15.2, 1:100, Biolegend, USA), in staining buffer supplemented with 3% normal mouse serum (Sigma-Aldrich, Germany) overnight at 4 °C in a humidity chamber. Samples were washed three times with PBS, and cell nuclei were labeled with Hoechst (Thermo Fisher Scientific, Carlsbad, CA) two drops per mL of PBS, according to the manufacturer's instructions. Slides were mounted in 50 µl/sample Floromount-G (Thermo Fisher Scientific, Carlsbad, CA) and were visualized using an Apotome microscope (Zeiss Observer 7).

Imaging analysis

Bioluminescence imaging

Bioluminescence analysis was performed as follows: To obtain peak values, the three highest fluxes within the post-injection imaging sequence were identified for each mouse at each time point, and the mean of these values was used as the representative bioluminescence value for that imaging session. These values were used to generate longitudinal tumor burden curves for individual mice as (integrated intensity +1) on a log10 scale and to compare groups. For correlation with histological tumor burden, the most recent bioluminescence measurement recorded before sacrifice was used as the endpoint.

Tumor burden analysis from H&E staining in QuPath

H&E images were acquired as a tile scan in the BX61 fluorescence microscope (Olympus, Germany) or Apotome (Zeiss, Germany). The Ome.tiff images were analyzed using QuPath 0.6.0. Briefly, a QuPath project was established with H&E images. First, for the Hematoxylin and Eosin channels, the estimate-stain-vectors function was applied to unify background values. To avoid bias and automate analysis, we trained the pixel classifier to annotate the background, tumor, and healthy lung tissue, as well as regions to exclude, such as folded regions with visible dirt. Particular attention was given to including bronchioles and vascular regions in the healthy lung annotation, since, due to their darker staining, the classifier often tags those regions as tumors. Then, with the annotated sample set, the 'train pixel classifier' ran with the following parameters: Classifier: Random Trees, resolution: moderate, Features: select channels: Eosin and Hematoxylin; set scale:2.0; select features: Gaussian and weighted Gaussian. The resulting classifier was saved. The classifier was applied to the entire project to generate full-image annotations, with a minimum of 50,000 and a maximum of 10^12. After validating the annotations, the tumor and tumor-free lung regions (in μm^2) were exported to an Excel spreadsheet. The rendered images containing the tumor annotations were saved. Tumor burden per mouse was calculated as follows:

$$\%\text{Tumor Burden} = \frac{Tumor\ um^2}{Tumor + tumor - free\ lung\ um^2} x100$$

Immunofluorescence image analysis

Lung lobe immunofluorescence tile-scan images were exported using the Zen 3.13 application (Zeiss). The immune cells in the TME were analyzed by QuPath 0.7.0. Briefly, the tumor and tumor-free regions were annotated based on H&E image analysis. For each region, cells were detected using the DAPI (Hoechst) channel.

$CD3^+$ T cells, $MHCII^+$ cells were defined as running object classifiers first for each channel, determining a positive signal, followed by creating composite classifiers for $Hoechst^+CD3^+$ and $Hoechst^+MHCII^+$. The rendered images and cell numbers corresponding to the classifiers were exported. The immune cell densities per tumor-free and within the tumor were calculated. Immune cell infiltration index was calculated for each $Hoescht^+CD3^+$ and $Hoechst^+MHCII^+$ as:

$$\text{Immune cell infiltration index} = \frac{immune\ cells\ per\ mm^2\ in\ tumor - free\ lung}{immune\ cells\ per\ mm^2\ in\ tumor}$$

Statistical Analysis

Statistical analyses were performed in GraphPad Prism (version 8). Survival was analyzed using the Mantel–Cox (log-rank) test, and a survival curve was established. Bioluminescence imaging (BLI) data were expressed as (electron flux +1) to visualize on a log10 scale and analyzed using a mixed-effects ANOVA (REML), with each mouse as a repeated measure and fixed effects for inoculation route, time, and their interaction. Body weight changes were monitored over time and are presented descriptively. Tumor burden between experimental groups was compared using the Kruskal–Wallis test with Dunn's multiple-comparison test. Associations between histological tumor burden and BLI signal intensity or body weight change were assessed using Spearman's rank correlation. A p-value <0.05 was considered statistically significant.

Results

LL2-luc2 cancer cell inoculation via aspiration establishes orthotopic lung tumors

To establish an orthotopic lung tumor, we inoculated luciferase-conjugated Lewis Lung cancer cells (LL2-luc2) via aspiration (n = 6) or the intranasal route (n = 6). The intranasal inoculation route is included as a control, since many groups have used it as an efficient, non-invasive route to target the lungs.[27] We monitored the experimental mouse well-being and weight change three times per week to determine progress and the severity of the OLC. Additionally, tumor inoculation and growth are verified by weekly bioluminescence readings (Figure 1a). Mice that scored 3 on a 5-point well-being scale, adapted from murine sepsis scoring, or those that lost more than 20% of their starting weight, were sacrificed.[25] Once the mice reached the humane endpoint, we collected the lungs and stained them with H&E to verify tumor engraftment. The weight-change plot showed that tumor growth began to affect animal health around day 30 (Figure 1b).

Without intervention, the health of mice in the aspiration-based inoculation and one mouse from the i.n. tumor engraftment group declined. By day 40 post-inoculation, all mice in the aspiration group reached the humane endpoint (Mantel–Cox log-rank test, $p = 0.0033$) (Figure 1c), whereas all the mice in the i.n. group, except one, showed no signs of tumor-related distress.

Bioluminescence imaging detects tumor progression with delayed signal emergence

We determined tumor engraftment and subsequent growth by weekly bioluminescence readings. Figure 2a shows a representative image of mice from aspiration-inoculated, i.n. – inoculated and control groups. No consistent tumor-associated BLI signal was observed at days 5 or 12 post-inoculation. Starting on day 19 post-engraftment, we observed a low-level BLI signal that intensified exponentially (Figure 2b, $p < 0.0001$). On day 33 p.i. mean BLI was 10^4 e^-/s (Figure 2a, b). By day 40 p.i., mean BLI increased to 10^5 e^-/s (Figure 2a,b).

Endpoint histopathology evaluation is a reference standard for orthotopic tumor verification

To verify tumor seeding and quantify tumor burden, the lungs of experimental groups were collected and analyzed with H&E staining (Figures 2c, 2d, and Extended data Figure 1).[44] Histopathological examination demonstrated that the tumor is spindle-shaped, with fibrillar cells and anisokaryotic nuclei, eosinophilic cytoplasm, and irregular, hyperchromatic nuclei. Tumor growth is characterized by perivascular seeding, with progression toward areas of necrosis (Extended Data Figure 2).[44] Tumor burden was calculated as the percentage of tumor area relative to total lung area using digital pathology (Figure 2c). Using the QuPath software from Bankhead *et al.*,[28] we trained the classifier to identify tumors and distinguish them from bronchioles, pulmonary veins, and healthy lung tissue (Extended Data Figure 3).[44] Once we

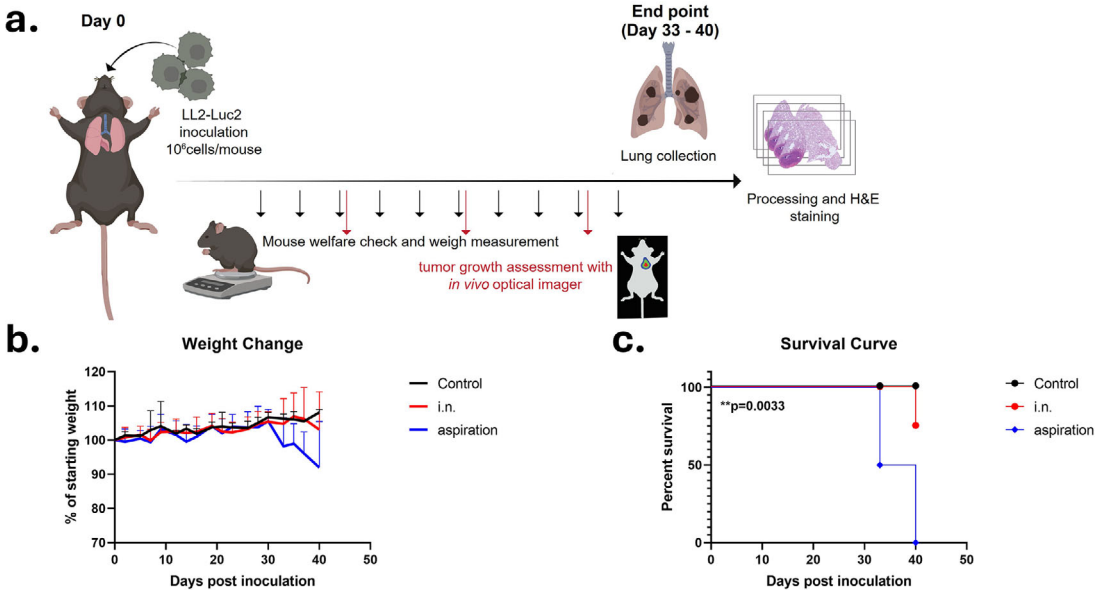


Figure 1. Inoculation of LL2-luc2 tumor cells by aspiration establishes orthotopic lung tumors. (a) Experimental timeline illustrating tumor cell inoculation, longitudinal monitoring, and endpoint analysis. (b) Body weight change is shown as a percentage of the starting weight for control (n = 5), i.n. (n = 6) and aspiration (n = 6) inoculation and presented descriptively, inferential statistics are not reported. (c) Kaplan–Meier survival curves of control (n = 5), intranasal inoculation (n = 6), and aspiration inoculation (n = 6) groups. Statistical significance was assessed using the Mantel–Cox (log-rank) tests.* $p < 0.05$; ** $p < 0.01$; *** $p < 0.001$.

differentiated healthy lung tissue from the tumor, we calculated the tumor burden (Figure 2d). Aspiration-based inoculation resulted in a significantly elevated tumor burden compared to the i.n. group. In i.n. tumor-inoculated group, only one mouse had successful tumor inoculation, consistent with the BLI signal (Figure 2). While endpoint pathological examination remains the reference standard for tumor verification, we analyzed the correlation between tumor burden and two commonly used indicators for tumor progression: weight loss and bioluminescence. The correlation between tumor burden and weight loss ($r = 0.7500$, $p = 0.066$) was stronger than that between tumor burden and bioluminescence ($r = 0.5714$, $p = 0.200$), but neither was statistically significant (Extended Data Fig 4).[44] Our results suggest that while BLI and weight loss reflect tumor progression, their correlation with quantitative tumor burden indicates that pathological examination remains the most reliable method for tumor assessment.

LL2-luc2 orthotopic tumors have limited immune cell infiltration

Solid tumors with minimal immune cell infiltration, immune-excluded tumors, are frequently associated with therapeutic resistance.[29] Thus, we analyzed immune cell infiltration in our successfully seeded tumors by aspiration. We stained lung sections from the experimental groups with MHC II and CD3 antibodies to identify dendritic cells/B cells and T cells, respectively. Our analysis clearly showed that immune cells were located at the tumor borders, with limited infiltration into the tumor core (Figure 3). Measuring the $MHCII^+$ and $CD3^+$ cells in tumor-free regions over within tumors, described here as the immune cell infiltration index, showed that tumor-free regions were enriched in $MHCII^+$ (2.26–3.68 fold) and $CD3^+$ (1.02–8.59 fold) cells (Figure 3e). Our findings demonstrate that aspiration-based inoculation of the LL2-luc2 cell line establishes tumors with a limited intratumoral immune cell infiltration, providing a valuable approach for studying therapies against treatment-resistant solid tumors.

Discussion

Reliable orthotopic cancer models in immunocompetent mice with minimal technical variability in tumor inoculation are essential for studies of preclinical tumor-microenvironment interaction. In this study, we established and characterized an aspiration-based tumor inoculation method that resulted in a successful tumor engraftment in all inoculated mice and reached a humane endpoint at day 33 to 40 post-inoculation. In contrast, intranasal inoculation resulted in significantly lower inoculation success (1/6), as confirmed by endpoint histopathology. Importantly, we also found that non-invasive tumor seeding via aspiration was associated with limited intratumoral immune cell infiltration, consistent with an immune-excluded-like tumor microenvironment. Altogether, the new method of inoculating lung tumors offers a practical, non-invasive, consistent, and reliable way to study the TME.

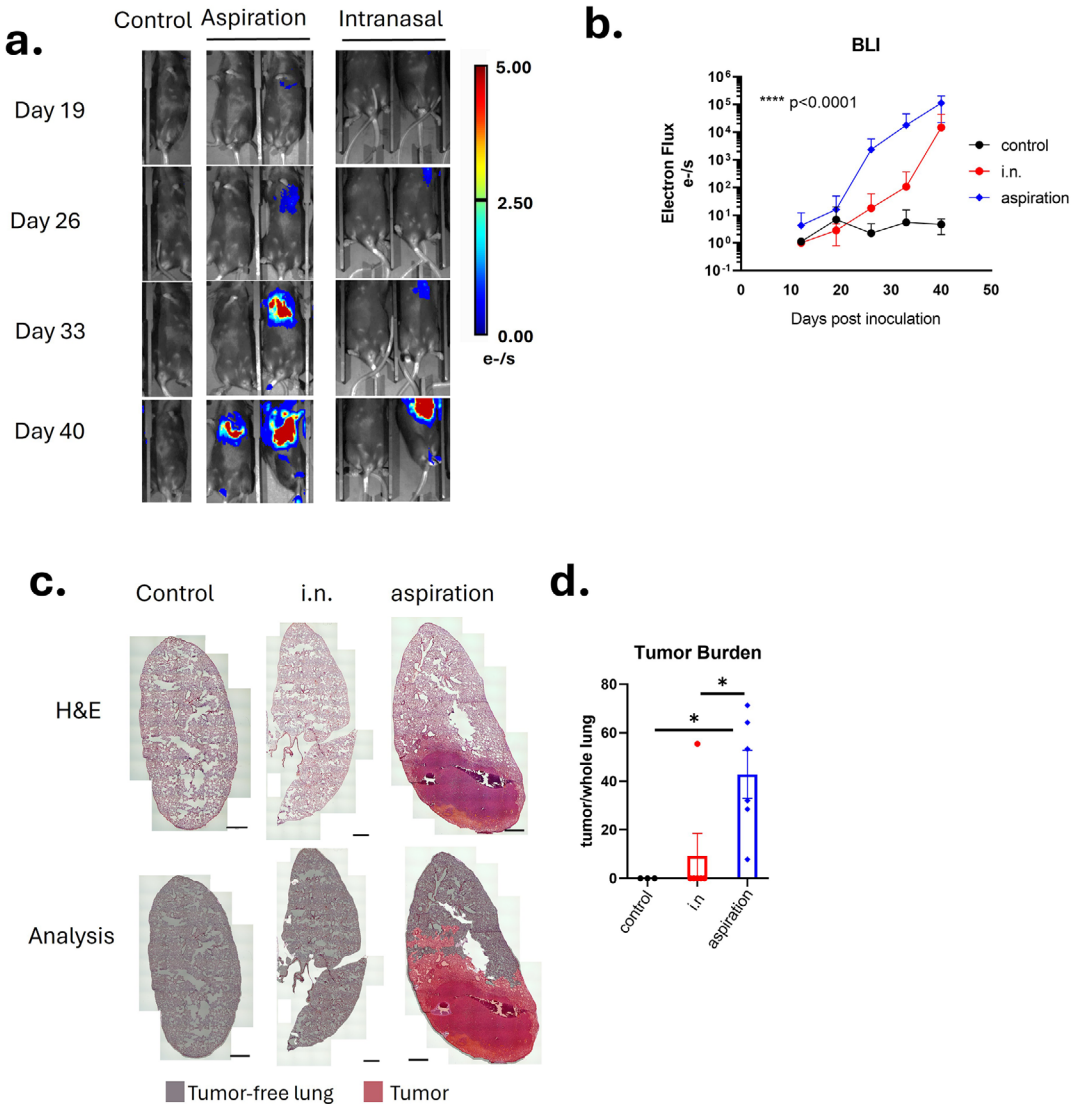


Figure 2. Bioluminescence imaging of tumor progression and pathological assessment of lung tumor burden. (a) Representative bioluminescence images of the control (n = 5), aspiration inoculation (n = 6), and intranasal inoculation (n = 6) groups, acquired 15 minutes after D-luciferin administration on days 19, 26, 33, and 40 post-inoculation. (b) Bioluminescence signal is expressed as electron flux (e−/s) + 1. Data are shown as mean ± SD on a log10 y-axis. BLI data were analyzed using a mixed-effects model to assess group and time effects. The p-value represents the time × inoculation interaction in the ANOVA mixed-effects models. (c) Representative lung sections stained with hematoxylin and eosin (upper panels) and corresponding tumor versus tumor-free lung region annotations obtained from QuPath analysis (lower panels) Scale bar 1 mm. (d) Tumor burden is quantified as a percentage of tumor area relative to total lung area. Data are shown as mean ± SD. Statistical significance was assessed using the Kruskal–Wallis test. * $p < 0.05$; ** $p < 0.01$; *** $p < 0.001$.

Intrathoracic/intrapulmonary injections[30–32] are commonly used methods to establish lung tumors. To provide a non-invasive alternative, Tanaka *et al.*[27] adapted the intranasal route that is commonly used in pulmonary infection studies to inoculate Lewis Lung cancer cells (LL2). The study compared the efficacy of inoculation to more traditional engraftment methods, intratracheal and intrapulmonary injection, side by side. The authors reported that i.n. inoculation more closely mimics the progression of primary human lung tumors, which originate from alveolar regions rather than from a random lung parenchymal region.[27] Building on this, we investigated whether aspiration, another respiratory delivery route frequently used to deliver biologics directly to the lung, could yield a consistent, reliable orthotopic lung tumor. We included a mock-inoculated control group and an intranasal engraftment group to compare the efficacy of our method with that reported in the current literature. We found that aspiration-based inoculation resulted in a significantly higher tumor incidence (6/6), whereas only 1 mouse in the intranasal group developed tumors (Figures 1 and 2). Survival in the

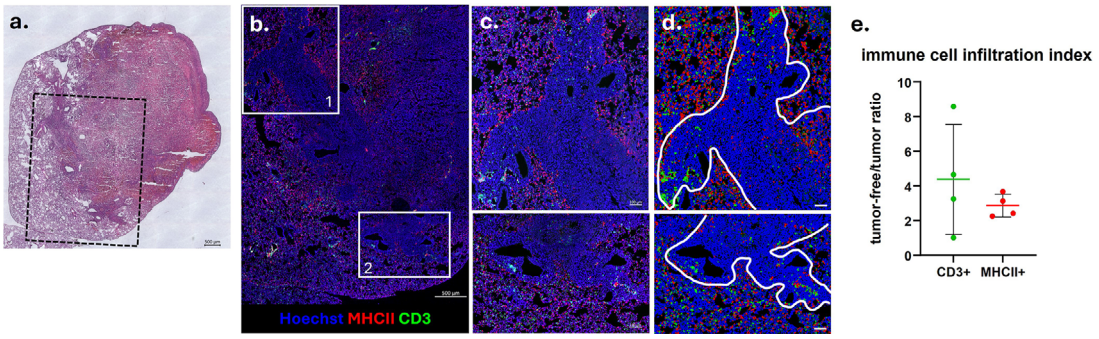


Figure 3. Immune cells located at the tumor borders in an aspiration-inoculated orthotopic lung cancer model. (a) Hematoxylin and eosin–stained lung section showing tumor localization. Scale bar 500 µm. **(b)** Consecutive sections were stained for Hoechst, CD3 (AF647), and MHCII (PE). The fluorescence image corresponds to the black dashed rectangle in H&E image at (a). Scale bar 500 µm. **(c)** Magnified images of the tumor–lung borders, localization of $CD3^+$ and $MHCII^+$ cells. Scale bar 100 µm. **(d)** QuPath cell annotations illustrating immune marker–positive cells within tumor and tumor-free lung regions. Scale bar 100 µm. **(e)** The ratio of $MHCII^+$ and $CD3^+$ immune cell densities to the tumor-free and tumor regions is represented as the immune cell infiltration index (n = 4).

aspiration group declined by day 30 post-inoculation, and all mice reached the humane endpoint by day 40 post-inoculation (Figure 1). LL2 was selected in our studies because LL2-induced tumors closely mimic human NSCLC,[33] including the TME,[22] have a relatively short doubling time in vitro, and are reported to contain a high proportion of cancer stem cells.[34]

Tumor aggressiveness is influenced by the inoculation dose.[27] In intrapulmonary lung cancer models, the number of inoculated cells ranged from 10^4 to $5x10^6$ cells/mouse.[30–32,35] The non-invasive inoculation routes, like i.n. and aspiration-based delivery are less precise than intrapulmonary inoculation. Tanaka *et al.* titrated the number of LLC cells. They found that mice receiving 10^7 cells/mouse died within 25 days post-inoculation, whereas 80% of mice inoculated with 10^6 cells/mouse survived, and all mice receiving the lowest concentration, 10^5 cells/mouse, survived.[27] Based on these findings, we selected 10^6 cells/mouse, yielding reproducible tumor establishment under our experimental conditions.

OLCs established by intrapulmonary injections exhibited rapid tumor progression; the bioluminescence signal emerged at day 5 post-inoculation,[31] and local tumor growth was detected as early as 2 weeks,[32] 3 weeks[30] post-inoculation. In contrast, in our aspiration model, we detected the BLI signal at 19 days post-inoculation (Figure 2) and small tumor seeds as early as 3 weeks post-inoculation, as shown by histopathology analysis. In previously reported intrapulmonary models, the OLC experimental group without intervention reached the endpoint within 10–20 days post-inoculation. Tumor growth in our model was approximately 2-fold slower, coinciding with the endpoint at 40 days post-inoculation (Figure 1). Overall, this slower progression provides an extended window for investigating tumor–TME interactions.

Monitoring orthotopic tumor growth by bioluminescence imaging signals and CT scans is a valuable tool. Studies report that BLI is often helpful for tracking tumor progression in orthotopic models,[36–38] but its correlation with true tumor burden is moderate and context-dependent.[4,39–41] A review of preclinical tumor models, either ectopic or orthotopic, that assess tumor growth by BLI found that BLI is strongly correlated with tumor burden in subcutaneous tumors, but this correlation weakens as tumors grow within body cavities.[38] Another study assessing the efficacy of BLI combined with MRI imaging of brain tumors in preclinical models found that early tumor progression is better reflected in BLI; however, the BLI vs. tumor burden curve plateaued due to hemorrhage and necrosis within the tumor that masked actual tumor severity, since BLI signals are coming from viable cells.[42] Another glioblastoma study focusing on complementary methods to monitor tumor burden reported that BLI alone showed poor correlation with tumor burden due to reduced tumor viability, necrosis, hypoxia, and instability of luciferase constructs within the growing tumor, which could be interpreted as regression.[40] Therefore, the tumor burden should be monitored using MRI combined with BLI. Similarly, in the orthotopic colon cancer model, the excised tumor weight correlated with MRI-derived tumor weight ($R^2 = 0.998$), whereas its correlation with BLI was poor ($R^2 = 0.57$).[39] Consistent with the literature, the limited linear correlation between bioluminescence signal and histologically quantified tumor burden in our study likely reflects the diffuse and multifocal nature of lung tumors, as well as the known limitations of BLI in capturing total tumor mass in the lung.

Immune exclusion represents a common barrier to effective anti-tumor immunity in solid cancers and remains underrepresented in highly inflamed preclinical models. In our study, we determined that our OLC has limited intratumoral immune cell infiltration; we quantified immune cells localized predominantly at the tumor borders (Figure 3), consistent with previous reports in which GFP-conjugated LLC cells were injected directly into the lung.[35] This spatial organization is consistent which demonstrate reduced intratumoral immune infiltration[43] compared to ectopic models[3,4] and reflects features commonly observed in human solid tumors.

This study has several limitations. The experimental group sizes were modest, and immune profiling was limited to selected markers to assess spatial distribution rather than comprehensive phenotyping. In addition, while BLI enabled longitudinal monitoring, quantitative tumor burden required endpoint histological analysis. Furthermore, the model was established using a single murine lung cancer cell line, and its applicability to other orthotopic lung cancer models remains to be determined.

In conclusion, we describe an aspiration-based syngeneic orthotopic lung cancer model that enables non-invasive and practical tumor establishment in immunocompetent mice. Compared with intranasal delivery, aspiration resulted in a markedly higher tumor inoculation rate and a consistent progression, while avoiding the technical complexity and tissue injury associated with intrapulmonary or intratracheal injection. Importantly, tumors established by aspiration exhibited a limited immune cell infiltration, with immune cells localized predominantly at tumor borders rather than within the tumor core. Together, these features position aspiration-based inoculation as easy to implement for orthotopic lung tumor modeling, particularly well-suited for preclinical studies of immune context- and microenvironment-targeted interventions.

Ethics and consent

All animal experimentation was approved by Izmir Biomedicine and Genome Center's internal animal experimentation ethics committee (on March 13, 2025, protocol # 2025–007). Animal experiments were conducted in accordance with national law and EU Directive 2010/63/EU. The study did not involve human participants or tissue of human origin thus consent was not applicable.

Data availability statement

All data supporting the findings of this study are available within the paper and its Extended data. Also, the record was deposited in Zenodo: Aspiration-induced orthotopic lung cancer model: a non-invasive method for in vivo tumor microenvironment studies (DOI:10.5281/zenodo.21903877).[44]

The record contains raw data and statistical analyses, mouse-level information, Extended Data Figure 1, Figure 2, Figure 3 and Figure 4, Extended Data Table 1, Table 2 and the completed ARRIVE 2.0 author checklist.

Extended Data Fig 1. H&E-stained lung sections (upper panel) and QuPath analysis (lower panel) of the samples classified as tumor vs. tumor-free regions. Scale bar 1 mm.

Extended Data Fig 2. Representative images of lung tumors to investigate tumor morphology. Tumor border (scale bar 200 μm) **(a)**, perivascular (within blue line) (scale bar 100 μm) **(b)**, and necrotic (scale bar 200 μm) **(c)** tumor regions.

Extended Data Fig 3. QuPath analysis flow

Extended Data Fig 4. The association between the terminal bioluminescence signal **(a)** or weight loss **(b)** and histologically quantified tumor burden was evaluated using a two-tailed Spearman rank correlation test.

Extended Data Table 1. Mouse welfare scoring system used for animal monitoring and humane endpoint assessment.

Extended Data Table 2. Reagents, suppliers, and catalogue identifiers used in the study.

The files are publicly available under a CC BY 4.0 license.

Acknowledgment

We would like to thank Professor Serap Birincioğlu for her evaluation of tumor H&E samples, core facility specialist Aslı Seren from the optical imaging unit for her assistance with imaging troubleshooting, and Ece Uzun from the histopathology unit for H&E staining of lung sections. We would also like to extend our gratitude to the animal caretakers,

Hamide Kaytaz and Hanim Güla, and the vivarium technicians, Burcu Kara, İbrahim Sevim, and Ulaş Saçıntı, for caring for the animals and for their assistance during our time of need.

This publication was created by benefiting from the 2236-B Marie Sklodowska-Curie Actions (MSCA) Cofund Scholarship Programs Contribution Fund Program (TUBITAK project ID: 123C460) and Horizon Europe MSCA Cofund Postdoctoral Program (EU project ID: 101126492). Views and opinions expressed are, however, those of the author(s) only and do not necessarily reflect those of the European Union or TUBITAK. Neither the European Union nor the granting authority can be held responsible for them.

References

1. Lamplugh ZL, Wellhausen N, June CH, *et al.*: **Microenvironmental regulation of solid tumour resistance to CAR T cell therapy.** *Nature Reviews Immunology. Nature Research.* 2025; **26**: 230–248.
PubMed Abstract | Publisher Full Text

2. Stribbling SM, Beach C, Ryan AJ: **Orthotopic and metastatic tumour models in preclinical cancer research.** *Pharmacol. Ther.* 2024; **257**. Elsevier Inc.
PubMed Abstract | Publisher Full Text | Free Full Text

3. Snipstad S, Bremnes F, Dehli Haugum M, *et al.*: **Characterization of immune cell populations in syngeneic murine tumor models.** *Cancer Med.* 2023; **12**: 11589–11601.
PubMed Abstract | Publisher Full Text | Free Full Text

4. Mao M, Qiu K, Feng L, *et al.*: **Immunological dynamics in orthotopic compared with subcutaneous murine models of HPV-positive oropharyngeal cancer.** *Dis. Model. Mech.* 2025; **18**: 18.
PubMed Abstract | Publisher Full Text | Free Full Text

5. Leiter A, Veluswamy RR, Wisnivesky JP: **The global burden of lung cancer: current status and future trends.** *Nat. Rev. Clin. Oncol.* 2023; **20**: 624–639. Springer Nature.
Publisher Full Text

6. National Institute of Health Surveillance E and ERP (SEER): **Cancer Stat Facts: Lung and Bronchus Cancer.**
Reference Source

7. Reck M, Frost N, Peters S, *et al.*: **Treatment of NSCLC after chemoimmunotherapy — are we making headway?.** *Nat. Rev. Clin. Oncol.* 2025; **22**: 806–830. Springer Nature.
Publisher Full Text

8. Sorin M, Rezanejad M, Karimi E, *et al.*: **Single-cell spatial landscapes of the lung tumour immune microenvironment.** *Nature.* 2023; **614**: 548–554.
PubMed Abstract | Publisher Full Text | Free Full Text

9. Zhang H, AbdulJabbar K, Moore DA, *et al.*: **Spatial Positioning of Immune Hotspots Reflects the Interplay between B and T Cells in Lung Squamous Cell Carcinoma.** *Cancer Res.* 2023; **83**: 1410–1425.
PubMed Abstract | Publisher Full Text | Free Full Text

10. Wang Y, Zhou H, Ju S, *et al.*: **The solid tumor microenvironment and related targeting strategies: a concise review.** *Front. Immunol.* 2025; **16**. Frontiers Media SA.
PubMed Abstract | Publisher Full Text | Free Full Text

11. Oser MG, MacPherson D, Oliver TG, *et al.*: **Genetically-engineered mouse models of small cell lung cancer: the next generation.** *Oncogene.* 2024; **43**: 457–469. Springer Nature.
Publisher Full Text

12. Gazdar AF, Hirsch FR, Minna JD: **From mice to men and back: An assessment of preclinical model systems for the study of lung cancers.** *J. Thorac. Oncol.* 2016; **11**: 287–299. Lippincott Williams and Wilkins.
Publisher Full Text

13. Woo XY, Srivastava A, Mack PC, *et al.*: **A Genomically and Clinically Annotated Patient-Derived Xenograft Resource for Preclinical Research in Non-Small Cell Lung Cancer.** *Cancer Res.* 2022; **82**: 4126–4138.
PubMed Abstract | Publisher Full Text | Free Full Text

14. Huo KG, D'Arcangelo E, Tsao MS: **Patient-derived cell line, xenograft and organoid models in lung cancer therapy.** *Transl Lung Cancer Res.* 2020; **9**: 2214–2232.
PubMed Abstract | Publisher Full Text | Free Full Text

15. Tanaka R, Yoshinouchi S, Karouji K, *et al.*: **A mouse model of lung cancer induced via intranasal injection for anticancer drug screening and evaluation of pathology.** *FEBS Open Bio.* 2023; **13**: 51–59.
PubMed Abstract | Publisher Full Text | Free Full Text

16. Gregório AC, Fonseca NA, Moura V, *et al.*: **Inoculated cell density as a determinant factor of the growth dynamics and metastatic efficiency of a breast cancer murine model.** *PLoS One.* 2016; **11**: 11.
PubMed Abstract | Publisher Full Text | Free Full Text

17. Greenlee JD, King MR: **A syngeneic MC38 orthotopic mouse model of colorectal cancer metastasis.** *Biol Methods Protoc.* 2022; **7**: 7.
PubMed Abstract | Publisher Full Text | Free Full Text

18. Chen C, Neumann J, Kühn F, *et al.*: **Establishment of an endoscopy-guided minimally invasive orthotopic mouse model of colorectal cancer.** *Cancers (Basel).* 2020; **12**: 1–16.
PubMed Abstract | Publisher Full Text | Free Full Text

19. Lee SB, Jeon HJ, Hyun H, *et al.*: **Establishment of an Orthotopic and Metastatic Colorectal Cancer Mouse Model Using a Tissue Adhesive-Based Implantation Method.** *Cancers (Basel).* 2025; **17**: 17.
PubMed Abstract | Publisher Full Text | Free Full Text

20. Rovers S, Farahmand P, Liu D, *et al.*: **A Minimally Invasive Transthoracic Injection Technique for Reproducible Intrapleural Delivery in Mice.** *Methods Protoc.* 2025; **8**: 8.
PubMed Abstract | Publisher Full Text | Free Full Text

21. Xu JJ, Lucero MY, Herndon NL, *et al.*: **Comparison of a Minimally Invasive Transthoracic Approach and a Surgical Method for Intrapleural Injection of Tumor Cells in Mice.** *Comp. Med.* 2023; **73**: 120–126.
PubMed Abstract | Publisher Full Text | Free Full Text

22. Yamada-Hara M, Takahashi N, Byun JW, *et al.*: **In Vivo Bioluminescence Imaging of Tumor Progression in the Lewis Lung Carcinoma Orthotopic Mouse Model: A Comparison Between the Tail Vein Injection and Intranasal Instillation Methods.** *Curr Protoc.* 2024; **4**: e70071.
PubMed Abstract | Publisher Full Text | Free Full Text

23. Anselmo AC, Gokarn Y, Mitragotri S: **Non-invasive delivery strategies for biologics.** *Nat. Rev. Drug Discov.* 2018; 19–40. Nature Publishing Group.
Publisher Full Text

24. Kinaret P, Ilves M, Fortino V, *et al.*: **Inhalation and Oropharyngeal Aspiration Exposure to Rod-Like Carbon Nanotubes Induce Similar Airway Inflammation and Biological Responses in Mouse Lungs.** *ACS Nano.* 2017; **11**: 291–303.
PubMed Abstract | Publisher Full Text

25. Shrum B, Anantha RV, Xu SX, *et al.*: **A robust scoring system to evaluate sepsis severity in an animal model.** *BMC. Res. Notes.* 2014; **7**: 7.
PubMed Abstract | Publisher Full Text | Free Full Text

26. Özkan M, Eskiocak YC, Wingender G: **Macrophage and dendritic cell subset composition can distinguish endotypes in adjuvant-induced asthma mouse models.** *PLoS One.* 2021; **16**: e0250533–e0250519.
PubMed Abstract | Publisher Full Text | Free Full Text

27. Tanaka R, Yoshinouchi S, Karouji K, *et al.*: **A mouse model of lung cancer induced via intranasal injection for anticancer drug screening and evaluation of pathology.** *FEBS Open Bio.* 2023; **13**: 51–59.
PubMed Abstract | Publisher Full Text | Free Full Text

28. Bankhead P, Loughrey MB, Fernández JA, *et al.*: **QuPath: Open source software for digital pathology image analysis.** *Sci. Rep.* 2017; **7**: 16878.
PubMed Abstract | Publisher Full Text | Free Full Text

29. Wu B, Zhang B, Li B, *et al.*: **Cold and hot tumors: from molecular mechanisms to targeted therapy.** *Signal Transduct. Target. Ther.* 2024; **9**: 274. Springer Nature.
PubMed Abstract | **Publisher Full Text** | **Free Full Text**

30. Gan W, He YM, Hu FL, *et al.*: **Establishment of an orthotopic model of lung cancer by transthoracic lung puncture using tumor fragments.** *J. Thorac. Dis.* 2023; **15**: 2012–2021.
PubMed Abstract | **Publisher Full Text** | **Free Full Text**

31. Tran Chau V, Liu W, Gerbé de Thoré M, *et al.*: **Differential therapeutic effects of PARP and ATR inhibition combined with radiotherapy in the treatment of subcutaneous versus orthotopic lung tumour models.** *Br. J. Cancer.* 2020; **123**: 762–771.
PubMed Abstract | **Publisher Full Text** | **Free Full Text**

32. Poczobutt JM, De S, Yadav VK, *et al.*: **Expression Profiling of Macrophages Reveals Multiple Populations with Distinct Biological Roles in an Immunocompetent Orthotopic Model of Lung Cancer.** *J. Immunol.* 2016; **196**: 2847–2859.
PubMed Abstract | **Publisher Full Text** | **Free Full Text**

33. He Q, Sun C, Pan Y: **Whole-exome sequencing reveals Lewis lung carcinoma is a hypermutated Kras/Nras–mutant cancer with extensive regional mutation clusters in its genome.** *Sci. Rep.* 2024; **14**: 14.
PubMed Abstract | **Publisher Full Text** | **Free Full Text**

34. Wang J, Sun Z, Liu Y, *et al.*: **Comparison of tumor biology of two distinct cell sub-populations in lung cancer stem cells.** 2017; **8**: 96852–96864.
PubMed Abstract | **Publisher Full Text** | **Free Full Text** | **Reference Source**

35. Weiss ID, Ella E, Dominsky O, *et al.*: **In the hunt for therapeutic targets: Mimicking the growth, metastasis, and stromal associations of early-stage lung cancer using a novel orthotopic animal model.** *J. Thorac. Oncol.* 2015; **10**: 46–58.
PubMed Abstract | **Publisher Full Text**

36. Klerk CPW, Overmeer RM, Niers TMH, *et al.*: **Validity of bioluminescence measurements for noninvasive in vivo imaging of tumor load in small animals.** *BioTechniques.* 2007; **43**: 7–13, 30.
PubMed Abstract | **Publisher Full Text**

37. Tuli R, Surmak A, Reyes J, *et al.*: **Development of a novel preclinical pancreatic cancer research model: Bioluminescence image-guided focal irradiation and tumor monitoring of orthotopic xenografts.** *Transl. Oncol.* 2012; **5**: 77–84.
PubMed Abstract | **Publisher Full Text** | **Free Full Text**

38. Shen YT, Asthana R, Peeters C, *et al.*: **Potential Limitations of Bioluminescent Xenograft Mouse Models: A Systematic Review.** *J Pharm Pharm Sci (www.cspsCanada.org).* 2020; **23**: 177–199.
PubMed Abstract | **Publisher Full Text** | **Reference Source**

39. Ravoori MK, Margalit O, Singh S, *et al.*: **Magnetic Resonance Imaging and Bioluminescence Imaging for Evaluating Tumor Burden in Orthotopic Colon Cancer.** *Sci. Rep.* 2019; **9**: 6100.
PubMed Abstract | **Publisher Full Text** | **Free Full Text**

40. Le TNT, Lim H, Hamilton AM, *et al.*: **Characterization of an Orthotopic Rat Model of Glioblastoma Using Multiparametric Magnetic Resonance Imaging and Bioluminescence Imaging.** *Tomography.* 2018; **4**: 55–65.
Publisher Full Text

41. Sechrist ZR, Lee G, Schwarz EM, *et al.*: **Validation of dual energy X-ray absorptiometry for longitudinal quantification of tumor burden in a murine model of pancreatic ductal adenocarcinoma.** *PLoS One.* 2024; **19**: e0292196.
PubMed Abstract | **Publisher Full Text** | **Free Full Text**

42. Jost SC, Collins L, Travers S, *et al.*: **Measur ing brain tumor growth: Combined bioluminescence imaging-magnetic resonance imaging strategy.** *Mol. Imaging.* 2009; **8**: 245–253.
PubMed Abstract | **Publisher Full Text** | **Free Full Text**

43. Na M, Kang H, Kim N, *et al.*: **Characterization of an orthotopic mouse transplant model reveals early changes in the tumor microenvironment of lung cancer.** *BMB Rep.* 2024; **57**: 484–489.
PubMed Abstract | **Publisher Full Text** | **Free Full Text**

44. Özkan M, Evcili İ, Güngör B: Aspiration-induced orthotopic lung cancer model: a non-invasive method for in vivo tumor microenvironment studies. [Dataset]. *Zenodo.* 2026.
Publisher Full Text

Open Peer Review

Current Peer Review Status: ?

Version 1

Reviewer Report 10 October 2026

https://doi.org/10.21956/openreseurope.27015.r82754

© **2026 Chan H.** This is an open access peer review report distributed under the terms of the Creative Commons Attribution License, which permits unrestricted use, distribution, and reproduction in any medium, provided the original work is properly cited.

?

Ho Wan Chan
[1] The University of Hong Kong, Pokfulam, China
[2] King's College London Institute of Pharmaceutical Science (Ringgold ID: 206990), London, England, UK

This article reports the development of an orthotopic lung cancer model induced by oropharyngeal aspiration of Lewis lung carcinoma (LLC) cells into the oropharynx for *in vivo* tumour microenvironment studies. The manuscript is generally well written with fairly detailed methodology, clear data presentation and clearly stated limitations. However, improvements should be made to the overall review and interpretation of the current literature, data presentation and interpretation of the bioluminescence imaging data, and awareness of possible confounding factors that may result in inaccurate comparisons between orthotopic models of lung cancer using intranasal administration, oropharyngeal aspiration, and other routes of administering lung cancer cells.

Introduction

1. The authors claimed in the abstract and Introduction section that oropharyngeal aspiration enables "consistent" tumour establishment. This term should be used carefully, as the inoculation success rate depends on sample size. The inoculation success rate of syngeneic orthotopic models was reported to be generally >90% at large sample sizes (n > 30)[1,2], so it would be more appropriate to avoid overstating the success rate considering the modest experimental group sizes (which the authors rightly highlighted as a limitation of the study in the Discussion section).

2. In the first paragraph of the Introduction section, the authors cited studies comparing the immune profile of other cancer types, e.g., oropharyngeal squamous cell carcinoma and colon cancer. Similar studies for lung cancer have been published[3,4] and should preferably be discussed over studies of other cancer types.

3. The authors claimed in the Introduction section that "Yet whether this approach can reliably deliver viable tumour cells to establish orthotopic lung tumours has not been investigated.

Consequently, there is currently no validated aspiration-based orthotopic lung cancer model for studies of tumour progression and the tumour microenvironment." This is invalid, as a recent study by Bardet et al.[4] also established a murine orthotopic lung adenocarcinoma model via oropharyngeal aspiration of LLC-Thy1.1 cells with detailed immune profiling (even though Bardet et al. named the technique "intratracheal direct method"). Please ensure that the current literature is thoroughly reviewed in the Introduction section.

4. The authors stated that the intratracheal and intrapulmonary injections introduce operator-dependent variability. Please explain why operator-dependent variability was less significant with oropharyngeal aspiration, given the high variation in tumour burden observed in the model developed in this study (Fig. 2(c)), which also fails to support the model's ability to overcome the challenge of variability in tumour size within experimental groups described by the authors.

Methods

1. In the "Animals" subsection, the authors stated that "the sample size was calculated according to the 3R rule and the experience of the lead researcher." This statement is vague; the authors should provide detailed sample size calculations based on the expected effect size and power.

2. Please explain why five female and one male mouse were used for the intranasal (i.n.) and aspiration groups; while sex differences are not the focus of this study, it is usually expected that half the mice would be male and half would be female. It would also be ideal to highlight how sex differences in tumour growth could potentially affect the results, especially immune cell infiltration.

3. Please state the cell passage number used in this study and whether the cells were checked for mycoplasma contamination in the "Luciferase-conjugated Lewis lung cancer cell maintenance and storage" subsection.

4. In the "*In vivo* orthotopic lung cancer model" subsection, the authors stated that "Prior to inoculation, the luciferase activity of LLC-luc2 cells was verified *in vitro*." Please explain the verification methodology in detail and provide relevant data (e.g., correlation between cell number and *in vitro* bioluminescence readings[1]). Please also clarify how many mice were used in the intranasal and aspiration PBS control groups and clearly define the region of interest.

5. In the "immunofluorescence" subsection, please state the blocking duration, the composition of the "staining buffer", and the type (33258 vs 33342) of Hoechst stain used.

6. The methodology for tumour burden and immunofluorescence analysis requires more explanation. Which image set and how many images were used to train the pixel classifier? What does the metric with a minimum of 50,000 and a maximum of 10^{12} refer to? For the % tumour burden calculation formula, why is the denominator "Tumour + tumour - free lung μm^2" (i.e., the tumour area was doubled)? The parameters for the object classifiers (alongside the pixel classifier) should also be stated.

Results and Discussion

1. A *p*-value of 0.0033 from the Mantel-Cox log-rank test could only indicate that there were

statistically significant between-group differences in survival probability, without specifically indicating whether the difference in survival probability between the i.n. and oropharyngeal aspiration groups was statistically significant. The authors are advised to conduct pairwise log-rank tests with Bonferroni correction.

2. The authors expressed the bioluminescence imaging data as (electron flux +1) in the subsection "Bioluminescence imaging detects tumour progression with delayed signal emergence" and Fig. 2(a)&(b), which is confusing in its meaning and is not a common readout employed to report bioluminescence imaging data. Furthermore, the electron flux values are surprisingly low compared to the usual flux values observed in other studies[1]. The authors are strongly advised to report the exact total flux values over the region of interest.

3. The results in Figure 2(d) showed that only 1 out of 6 mice in the i.n. group had successful tumour inoculation (as determined by tumour area), which differs significantly from the results reported by Tanaka et al.[5], wherein tumour was successfully inoculated in all mice after i.n. administration of the same number of LLC cells, i.e., 10^6 (albeit with a small tumour area). Please compare and discuss such differences.

4. There were several confounding factors that may explain poor correlation between bioluminescence imaging data and tumour burden. Firstly, performing bioluminescence imaging in the lateral position resulted in greater correlation with computed tomography-derived tumour volume than the ventral position (which was used in this study), as reported in Picabeta et al.[3]. Secondly (and perhaps more importantly), why was fur depilation not conducted? Melanin in fur is well known to quench bioluminescence signals with significant biological and temporal variation[6], and may explain the weak signals observed with bioluminescence imaging and its poor correlation with tumour burden assessed by tumour area quantification of H&E-stained tissue sections. It is generally expected that depilation be done for dark-furred mice (e.g., C57BL/6J mice)undergoing *in vivo* bioluminescence imaging studies. Furthermore, endpoint *ex vivo* fluorescent imaging and lung weight measurements would also be useful readouts of quantitative tumour burden without the need for further tissue processing.

5. Could the chosen method of anaesthesia confound the results observed in this study? A previous study by Seo et al.[7] showed that the use of isoflurane anaesthesia resulted in i.n. doses sometimes bubbling back out of the nares of mice and a lower pulmonary delivery efficiency ~(30%) compared to ketamine/xylazine anaesthesia (~50%), while pulmonary dosing efficiency using oropharyngeal aspiration is not altered by anaesthetic type (~60%). It is likely that if ketamine/xylazine anaesthesia was applied in lieu of isoflurane anaesthesia, more mice would be engrafted with tumour after i.n. administration, as more cells would be delivered to the lungs (even if the inoculation rate would likely still be lower due to pulmonary delivery efficiency of i.n. administration anaesthesia being lower than that of oropharyngeal aspiration under ketamine/xylazine anaesthesia).

6. The authors stated in the Discussion section that the study by Tanaka et al.[5] reported that i.n. inoculation more closely mimics the progression of primary human lung tumours, which originate from alveolar regions rather than from a random lung parenchymal region. Firstly, the lung parenchyma practically comprises mostly respiratory bronchioles and alveoli (which Tanaka et al.[5] observed tumour formation around), so it is confusing that the authors claim that the tumour originates from alveolar regions rather than from a random lung parenchymal region (this point

was not discussed by Tanaka et al.[5]). Secondly, it is questionable whether i.n. inoculation and especially oropharyngeal aspiration truly more closely mimic the progression of primary lung cancers. Oropharyngeal aspiration is known to deliver compounds to both lungs (refer to Fig. 3(a) of Seo et al.[7]), and it is likely that aspiration of cancer cells would result in their diffuse spreading to both lungs, similar to intratracheal administration, which would result in the formation of multiple synchronous tumours and interfere with progression and lung metastasis processes[8].

7. In the Discussion section, the sentence "This spatial organization is consistent which demonstrate reduced intratumoral immune infiltration compared to ectopic models and reflects features commonly observed in human solid tumors." seems to be incomplete. Also, please consider the results from Picabea et al.[3], which show increased immune infiltration compared with subcutaneous tumours.

8. For the dataset, please provide (1) raw mouse body weight data, (2) raw .czi images, and (3) raw bioluminescence imaging files with relevant metadata

References

1. Tanaka R, Yoshinouchi S, Karouji K, Tanaka Y, et al.: A mouse model of lung cancer induced via intranasal injection for anticancer drug screening and evaluation of pathology. *FEBS Open Bio*. 2023; **13** (1): 51-59 Publisher Full Text
2. Seo Y, Qiu L, Magnen M, Conrad C, et al.: Optimizing anesthesia and delivery approaches for dosing into lungs of mice. *American Journal of Physiology-Lung Cellular and Molecular Physiology*. 2023; **325** (2): L262-L269 Publisher Full Text
3. Bardet P, Allonsius L, Hadadi E, Kancheva D, et al.: Multiomics immune profiling of a patient-relevant orthotopic lung cancer model using SEPARATE-Seq. *Nature Communications*. 2026; **17** (1). Publisher Full Text
4. Picabea B, Orive D, Rodríguez C, Mailharin M, et al.: Establishment and characterization of an orthotopic implanted lung cancer model to mimic human tumor structure, microenvironment, and metastatic spread. *Translational Lung Cancer Research*. 2025; **14** (11): 4868-4895 Publisher Full Text
5. Peng L, Feng L, Yuan H, Benhabbour S, et al.: Development of a novel orthotopic non-small cell lung cancer model and therapeutic benefit of 2′-(2-bromohexadecanoyl)-docetaxel conjugate nanoparticles. *Nanomedicine: Nanotechnology, Biology and Medicine*. 2014; **10** (7): 1497-1506 Publisher Full Text
6. Nakajima T, Anayama T, Matsuda Y, Hwang D, et al.: Orthotopic Lung Cancer Murine Model by Nonoperative Transbronchial Approach. *The Annals of Thoracic Surgery*. 2014; **97** (5): 1771-1775 Publisher Full Text
7. Curtis A, Calabro K, Galarneau J, Bigio I, et al.: Temporal Variations of Skin Pigmentation in C57Bl/6 Mice Affect Optical Bioluminescence Quantitation. *Molecular Imaging and Biology*. 2011; **13** (6): 1114-1123 Publisher Full Text
8. Mordant P, Loriot Y, Lahon B, Castier Y, et al.: Bioluminescent Orthotopic Mouse Models of Human Localized Non-Small Cell Lung Cancer: Feasibility and Identification of Circulating Tumour Cells. *PLoS ONE*. 2011; **6** (10). Publisher Full Text

Is the work clearly and accurately presented and does it cite the current literature?
Partly

Is the study design appropriate and does the work have academic merit?

Partly

Are sufficient details of methods and analysis provided to allow replication by others?
Partly

If applicable, is the statistical analysis and its interpretation appropriate?
Partly

Are all the source data underlying the results available to ensure full reproducibility?
Partly

Are the conclusions drawn adequately supported by the results?
Partly

Competing Interests: No competing interests were disclosed.

Reviewer Expertise: Pulmonary drug delivery, respiratory disease model development, nanomedicine, extracellular vesicles

I confirm that I have read this submission and believe that I have an appropriate level of expertise to confirm that it is of an acceptable scientific standard, however I have significant reservations, as outlined above.